Mesh Resolution Impacts the Accuracy of Inverse and Forward ECG Problems

Bing Yao, Shenli Pei, Hui Yang, *Member, IEEE*

***Abstract*—Electrocardiographic imaging (ECGI) has become an important medical diagnosis tool that assists scientists to noninvasively investigate cardiac electric activity. Many previous works have studied the inverse and forward ECG problems to understand how to reconstruct the cardiac electric activity from the body potential distribution. However, the inverse ECG problem is highly ill-conditioned and very sensitive to errors and noises. Thus, there is a need to study the sensitivity of inverse and forward ECG problems. In this paper, we investigated effects of mesh resolution on the accuracy of inverse and forward ECG problems. First, we employed the boundary element method to calculate the relationship between potential distributions on the body and heart surfaces and developed an algorithm to solve inverse and forward ECG problems. Second, we implemented the algorithm to solve the ECG problems in both a concentric spherical geometry and a realistic torso-heart geometry. Third, we evaluated the relative error between our solution and the analytical solution under the condition of different mesh resolutions. Experimental results explicitly show that the relative error in the inverse solution decreased from 30% to 17% when the mesh elements triangulating the two spheres increased from 24 to 400 in the concentric spherical geometry, and that decreased from 26% to 16% when the mesh elements triangulating the heart surface increased from 136 to 546 in the realistic torso-heart geometry.**

***Keywords*—ECG Inverse Problem, ECG Forward Problem, Boundary Element Method, Regularization, Mesh Resolution**

I. Introduction

Electrocardiographic imaging (ECGI) has emerged as a promising medical technology that empowers scientists to noninvasively investigate cardiac electric activities. Inverse and forward ECG problems are the theoretical background of ECGI. In the inverse ECG problem, electric potentials on the heart surface are estimated from the potential distribution on the torso surface, while in the forward ECG problem, the electric potentials on the body surface are computed from the potential distribution on the heart surface. The inverse and forward ECG methods have been proposed to diagnose the pathophysiological activity of the heart in many previous works. For example, the inverse electrocardiography has been implemented to image the cardiac potential distribution and it showed great potential to noninvasively detect the extent and location of myocardial infarction [1].

This work is supported in part by the National Science Foundation (CMMI-1617148, CMMI-1619648, and IOS-1146882).

Bing Yao, Shenli Pei and Hui Yang* are with the Complex System Monitoring, Modeling and Analysis Laboratory, The Pennsylvania State University, University Park, PA 16802 USA (*corresponding author: huy25@psu.edu)

However, the inverse ECG problem is highly ill-conditioned and very sensitive to errors and noises. Thus, it's challenging to precisely diagnose cardiac diseases based on the inverse model. In inverse and forward ECG problems, the key is to solve the tranfer matrix that characterizes the relationship between potential distributions on the heart and body surfaces. Solving the transfer matrix involves tackling the Laplace's equation in a source-free homogeneous volume conductor whose boundary is formed by the body and heart surfaces, which results in complicated surface integrations [2]. These integrations are only solvable in a tractable geometry such as a set of concentric spheres. To solve them in a realistic torso-heart geometry, boundary element method (BEM) has been widely employed [3] [4]. In this method, the torso and heart surfaces are discretized into meshes, and the integrals can be subdivided into a series of numerical integrations over mesh elements. The accuracy of numerical solutions is correlated with the mesh resolution in BEM. For that reason, there is an urgent need to study how mesh resolution impacts the accuracy of inverse and forward solutions of ECG problems.

The objective of this paper is to investigate effects of mesh resolution on the accuracy of inverse and forward solutions for ECG problems. First, we employed BEM to calculate the transfer matrix and developed an algorithm to solve the inverse and forward ECG problems. Second, we implemented the algorithm into both a concentric spherical geometry and a realistic torso-heart geometry. Finally, we investigated the model accuracy under different mesh resolutions. Experimental results showed that the accuracy of our solutions improves as the mesh resolution increases.

The organization of this paper is as follows: Section II describes the research methodology of our inverse and forward models; Section III presents the model implementation and experimental design; Section IV illustrates the experimental results under different mesh resolutions; Section VI concludes our study.

II. Research Methodology

In this section, we will first present the boundary element solution of the transfer matrix that characterizes the relationship between electric potentials on the body and heart surfaces. Second, we will introduce the methods based on the transfer matrix to solve the inverse and forward ECG problems. Specifically, Tikhonov zero-order regularization, which is employed in the highly ill-conditioned inverse problem, will be introduced.

A. Boundary Element Solution of the Transfer Matrix in Inverse and Forward ECG problems

We modeled the human body as a source-free homogeneous volume conductor whose boundary is formed by the body and heart surfaces S_B and S_H. The relationship between electric potentials on S_B and S_H can be represented by $\Phi_B = R_{BH}\Phi_H$, where R_{BH} is the transfer matrix, and Φ_B and Φ_H represent the potentials on S_B and S_H, respectively.

Calculating R_{BH} is the key point to solve the inverse and forward ECG problems. Divergence theorem and Green's Second Identity are employed to obtain R_{BH} [2]. Suppose a volume $V \subset R^3$ is compact and has a piecewise smooth boundary S; if F is a continuously differentiable vector field defined on a neighborhood of V, then according to Divergence theorem we have

$$\iiint_V (\nabla \cdot \vec{F})dV = \oiint_S (\vec{F} \cdot \hat{n})dS \tag{1}$$

where $\hat{n}$ is the unit normal vector of S pointing outward. If Φ and Ψ are both twice continuously differentiable on V, and choose $F = \Phi\nabla\Psi - \Psi\nabla\Phi$, according to Eq. (1), Green's second identity follows immediately

$$\oiint_S (\Phi\nabla\Psi - \Psi\nabla\Phi)\cdot\hat{n}\, dS = \iiint_V (\Phi\nabla^2\Psi - \Psi\nabla^2\Phi)\, dV \tag{2}$$

Let Φ be electric potentials and $\Psi = \frac{1}{r}$. Given that S_B and S_H are piecewise smooth, and the facts that $\nabla^2\Phi = 0$ between the two surfaces, and $\nabla\Phi = 0$ on S_B, according to Eq. (2) electric potentials on S_B and S_H are

$$\Phi_B{}^i = -\frac{1}{4\pi}\iint_{S_H}\Phi_H\, d\Omega_{BH}{}^i - \frac{1}{4\pi}\iint_{S_H}\frac{\nabla\Phi_H\cdot\hat{n}}{r^i}dS_H + \frac{1}{4\pi}\iint_{S_B}\Phi_B\Omega_{BB}{}^i \tag{3a}$$

$$\Phi_H{}^i = -\frac{1}{4\pi}\iint_{S_H}\Phi_H\, d\Omega_{HH}{}^i - \frac{1}{4\pi}\iint_{S_H}\frac{\nabla\Phi_H\cdot\hat{n}}{r^i}dS_H + \frac{1}{4\pi}\iint_{S_B}\Phi_B\Omega_{HB}{}^i \tag{3b}$$

where $d\Omega_{BH}$ denotes the solid angle subtended at a location on S_B by a mesh element on S_H. We then employed BEM to solve the integrals above. The torso and heart surfaces are discretized by triangular elements. Thus, each term in equation (3a) and (3b) can be discretized as:

$$A_{BB}\Phi_B + A_{BH}\Phi_H + M_{BH}N_H = 0 \tag{4a}$$

$$A_{BB}\Phi_B + A_{BH}\Phi_H + M_{BH}N_H = 0 \tag{4b}$$

The matrices, A's and M's depend entirely on the torso-heart geometry, where A_{BB}, A_{BH}, and M_{BH} denote the geometry coefficient matrices in which the observing locations are on the body surface, while A_{HB}, A_{HH}, and M_{HH} correspond to the matrices, where the observer stands on the heart surface. N_H contains the normal components of $\nabla\Phi_H$. Combining equations (4a) and (4b), we obtained the transfer matrix:

$$R_{BH} = (A_{BB} - M_{BH}M_{HH}^{-1}A_{HB})^{-1}(M_{BH}M_{HH}^{-1}A_{HH} - A_{BH}) \tag{5}$$

which is then employed to compute and estimate the body and cardiac potential distributions in forward and inverse ECG problems.

B. Tikhonov Zero-order Regularization

In the forward ECG problem, electric potentials Φ_H on the heart surface are given, and we can directly compute electric potentials Φ_B on the torso surface by $\Phi_B = R_{BH}\Phi_H$. However, in the inverse problem, although electric potentials Φ_B on the torso surface are provided, it's very complex to solve Φ_H directly, as R_{BH} may not be a square matrix and it's always highly ill-conditioned. Therefore, Tikhonov zero-order regularization [5] is adopted to obtain a stable solution for Φ_H in this paper.

Tikhonov zero-order regularization can be formulated as the solution of the following objective function:

$$\Phi_H = arg\min_{\Phi_H}\{J(\Phi_H) = \|R_{BH}\Phi_H - \Phi_B\|2 + \lambda^2\|\Phi_H\|^2\} \tag{6}$$

where $\|\cdot\|$ represents L2-norm, and λ is regularization parameter chosen by L-curve method [6], as shown in Fig. 4. The L-curve plot displays the trade-off between the fit to the given data and size of a regularized solution, as λ varies. The regularization parameter, λ, is often chosen to be the one that amounts to the corner of the L-curve plot. Taking the derivative of $J(\Phi_H)$ with respect to Φ_H and setting it to zero, gives the estimate of the inverse solution:

$$\hat{\Phi}_H = (R_{BH}^T R_{BH} + \lambda^2 I)^{-1}R_{BH}^T\Phi_B \tag{7}$$

where I is the identity matrix. Based on Eq. (7) and given the regularization parameter λ, we can estimate the cardiac potential distribution Φ_H in the inverse ECG problem.

III. Experimental Design

In this section, we implemented the algorithm developed in section II in both a concentric spherical geometry and a realistic torso-heart geometry. First, we solved the forward and inverse ECG problems in a concentric spherical geometry. Second, we employed our inverse model to estimate the cardiac potential distribution in a realistic torso-heart geometry. Third, three performance metrics are defined to characterize the accuracy of our model.

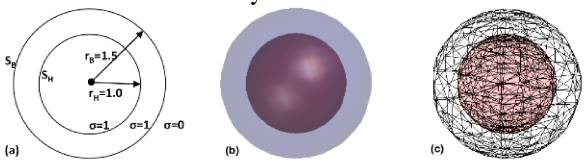

Fig. 1: (a) Radii and conductivity of the inner and outer spheres. Interpolated (b) and discretized (c) concentric spherical geometry.

A. Experiment in a Concentric Spherical geometry

The concentric spherical geometry studied here is shown in Fig. 1. The inner sphere behaves like the heart surface S_H, and the outer sphere represents the torso surface S_B. A current dipole-moment $\vec{p}$ was placed at the common center of S_H and S_B. Assume the conductivity outside S_B is zero and that inside S_B is σ. Then the electrical potentials produced by the current dipole at different observing locations on S_H and S_B [7] are

$$\Phi_H^i = \frac{1}{4\pi\sigma}\frac{\vec{p}\cdot\hat{r}_H^i}{r_B^2}\left[2\left(\frac{r_H}{r_B}\right) + \left(\frac{r_B}{r_H}\right)^2\right] \tag{8}$$

$$\Phi_B^i = \frac{3}{4\pi\sigma}\frac{\vec{p}\cdot\hat{r}_B^i}{r_B^2} \tag{9}$$

where, r_H and r_B are the radii of S_H and S_B, and $\hat{r}_H^i$ and $\hat{r}_B^i$ are the unit vectors from the center to the location i on S_H and S_B, respectively.

In the simulation, we set $\vec{p} = (10,10,10)$, $\sigma = 1$, $r_H = 1.0$, $r_B = 1.5$, and discretized S_H and S_B with two sets of

triangular elements. In the forward simulation, the potential Φ_H on the inner sphere is known by assumption and given by Eq. (8). Then, we calculated the potential Φ_B on the outer sphere by $\Phi_B = R_{BH}\Phi_H$. On the contrary, in the inverse simulation, Φ_B on the outer sphere is known by assumption and given by Eq. (9). By utilizing Eq. (7) we estimated Φ_H on the inner sphere.

B. *Experiment in a Realistic Torso-heart Geometry*

The algorithm is then implemented to solve the inverse ECG problem in a realistic torso-heart geometry, as shown in Fig. 2. The body-surface potential maps (BSPMs) are provided by the 2007 PhysioNet/Computers in Cardiology Challenge [8]. The BSPMs, denoted as Φ_B, come from interpolating the original body-surface ECGs recorded at 120 anatomical locations on the torso to 352 locations corresponding to the standard Dalhousie torso projected on the new customized torso geometry [1]. In this case, Φ_B are provided, and by utilizing Eq. (7), we estimated the potentials Φ_H on the heart surface.

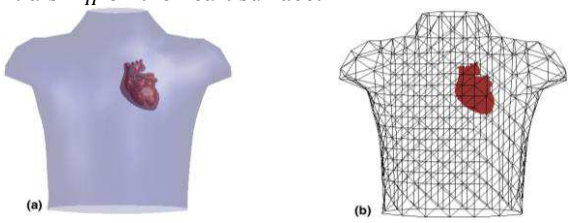

Fig. 2: (a) Interpolated (b) Discretized torso-heart geometry

C. *Performance Metrics*

Both the forward and inverse solutions were compared with analytical results that are directly computed or with real measured data. The accuracy is evaluated by mean squared error (MSE), relative error (RE) and correlation coefficient (CC) between the true potentials and estimated results. The three performance metrics are defined as follows:

$$MSE = \frac{1}{N}\sum_{i=1}^{N}(\Phi_i^{est} - \Phi_i)^2 \tag{11}$$

$$RE = \frac{\|\vec{\Phi}^{est} - \vec{\Phi}\|}{\|\Phi\|} \tag{12}$$

$$CC = \frac{E\left[(\vec{\Phi}^{est} - E(\vec{\Phi}^{est}))(\vec{\Phi} - E(\vec{\Phi}))\right]}{\|(\vec{\Phi}^{est} - E(\vec{\Phi}^{est}))\|\|\vec{\Phi} - E(\vec{\Phi})\|} \tag{13}$$

where $\vec{\Phi}^{est}$ represents the electric potentials estimated by our inverse and forward models, and $\vec{\Phi}$ denotes the true results. Function $E(x)$ represents the expectation or the average of x, and $\|\cdot\|$ represents L2-norm. The MSE characterizes the overall deviation, RE measures the deviation percentage, and CC is a measure of the spatial differences between the estimator and what is estimated.

IV. RESULTS

A. *Experimental Results of the Forward Model in the Concentric Spherical Geometry*

In the forward simulation, the estimated potentials $\vec{\Phi}_{B\_est}$ on the outer sphere are compared with the analytical potentials $\vec{\Phi}_B$. Table.1 shows the true electric potentials at seven different locations on the outer sphere and the estimated results when S_H and S_B are triangulated with 60 elements ($N = 60$) and 240 elements ($N = 240$). It can be noted that the estimated results are closer to true values when $N = 240$ than those when $N = 60$.

TABLE I. FORWARD RESULTS IN TWO-SPHERE SIMULATION

Coordinates	Φ_B	Φ_{B_est}(N=60)	Φ_{B_est}(N=240)
(0,0,1)	1.061	1.222	1.114
(-0.5,0,0.866)	1.449	1.586	1.475
(-0.433,0.75,0.5)	-0.725	-0.790	-0.737
(-1,0,0)	0.388	0.466	0.397
(0.433,-0.75,-0.5)	0.725	0.781	0.764
(0.5,0,-0.866)	-1.449	-1.654	-1.513
(0,0,-1)	-1.061	-1.219	-1.108

Fig. 3 shows the variations of MSE, RE, CC with the number of triangles in the forward simulation with the concentric spherical geometry. The number of triangles N discretizing S_H and S_B takes the values: 24, 60, 112, 180, 264, 364, 480, 612 and 760. Note that MSE (Fig. 3(a)) and RE (Fig. 3(b)) decrease, and CC (Fig. 3(c)) increases as N increases. All the three performance metrics converge when $N > 400$: MSE approaches zero; RE is less than 3% and converges to 1%; CC goes to 1.

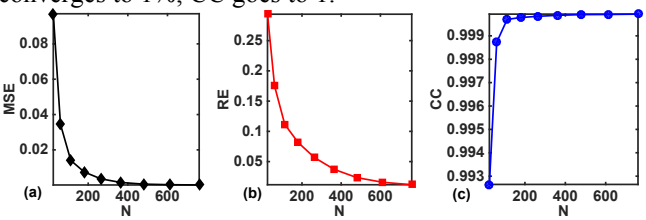

Fig. 3: The variation of (a) MSE (b) RE (c) CC with the number of triangles in the forward simulation of a concentric spherical geometry.

B. *Experimental Results of the Inverse Model in the Concentric Spherical Geometry*

In the inverse simulation, Tikhonov zero-order regularization was adopted to solve the electrical potentials Φ_H on the inner sphere. The regularization parameter λ is set to be 0.148 when $N = 60$, and 0.116 when $N = 240$ according to the L-curve study, as shown in Fig.4.

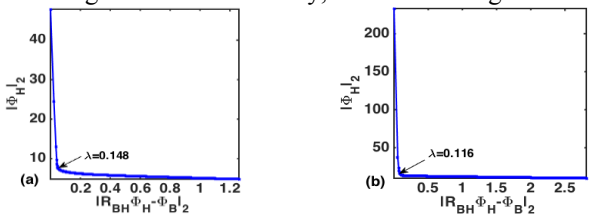

Fig. 4: L-curve plots when S_H and S_B are triangulated with (a) 60 triangles; (b) 240 triangles.

The estimated potentials $\vec{\Phi}_{H\_est}$ on the epicardial surface is compared with the true potentials $\vec{\Phi}_H$. Table.2 shows the true electric potentials and the estimated results at seven different locations on the inner sphere under two different mesh resolutions. Again, it can be noted that the estimated results are closer to the true values when $N = 240$ than those when $N = 60$.

The variations of MSE, RE, CC with number of triangles in the inverse simulation with the concentric spherical geometry are shown in Fig. 5. Similar to the forward

simulation, the number of triangles N discretizing S_H and S_B takes the values: 24, 60, 112, 180, 264, 364, 480, 612 and 760. Note that MSE (Fig. 3(a)) and RE (Fig. 3(b)) decrease, and CC (Fig. 3(c)) firstly increases and then oscillates around 0.986 as N increases. The performance metrics MSE and RE converge when $N > 400$: MSE converges to 0.01, RE approaches 17%.

TABLE II. INVERSE RESULTS IN TWO-SPHERE SIMULATION

Coordinates	Φ_H	$\Phi_{H\ est}$(N=60)	$\Phi_{H\ est}$(N=240)
(0,0,1)	1.267	1.040	1.171
(-0.5,0,0.866)	0.464	0.204	0.448
(-0.433,0.75,0.5)	1.035	1.002	0.918
(-1,0,0)	-1.267	-1.136	-1.248
(0.433,-0.75,-0.5)	-1.035	-0.544	-0.780
(0.5,0,-0.866)	-0.464	-0.316	-0.277
(0,0,-1)	-1.267	-1.070	-1.241

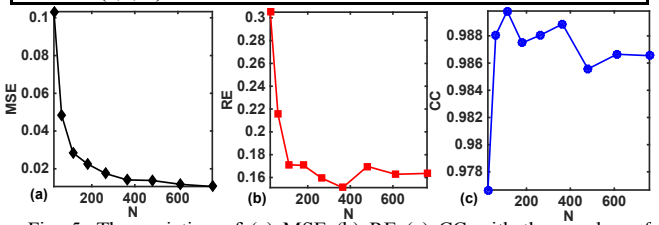

Fig. 5: The variation of (a) MSE (b) RE (c) CC with the number of triangles in the inverse simulation of a concentric spherical geometry.

C. *Experimental Results of the Inverse Model in a Realistic Torso-heart Geometry*

We implemented our inverse model to a realistic torso-heart geometry and estimated $\vec{\Phi}_{H\_est}$ on the heart surface from $\vec{\Phi}_B$ acquired on the body surface. After obtaining $\vec{\Phi}_{H\_est}$, we computed $\vec{\Phi}_{B\_est}$ on the torso surface by $\Phi_B = R_{BH}\Phi_H$, and compared them with the true data $\vec{\Phi}_B$. The number of triangles discretizing the realistic heart surface takes the values: 136, 272, 408, 546, 654, 872 and 1092. Fig. 6 is an illustration of the 3D heart model [9] and the triangulated heart surface.

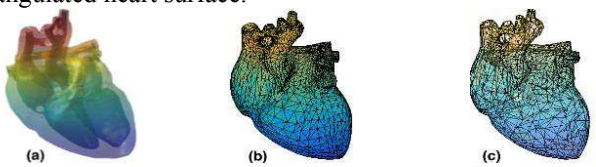

Fig. 6: (a) Interpolated (b) Meshed (c) Coarsely meshed heart surface.

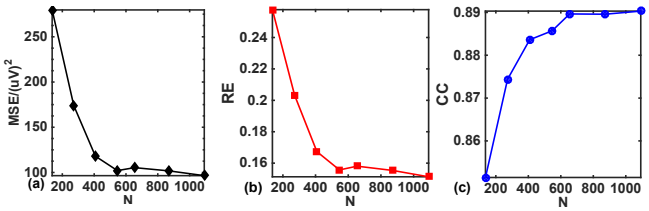

Fig. 7: The variation of (a) MSE (b) RE (c) CC when the number of triangles increases in a realistic torso-heart geometry.

The variations of MSE, RE and CC with number of triangles N discretizing the heart surface in the realistic torso-heart geometry are shown in Fig. 7. Note that MSE (Fig. 3(a)) and RE (Fig. 3(b)) decrease, and CC (Fig. 3(c)) increases as N increases, which is consistent with our simulation results in the concentric spherical geometry. Similarly, all the three performance metrics converge when $N > 600$: MSE approaches $1 \times 10^{-4}(mV)^2$, RE approaches 15%, and CC goes to 0.89.

V. CONCLUSIONS

In this paper, we developed an algorithm to solve inverse and forward ECG problems by using a transfer matrix. In the forward model, electrical potentials on the torso surface can be calculated directly by the relationship between potential distributions on the two surfaces. In the inverse model, Tikhonov zero-order regularization is employed to obtain a stable solution for cardiac electric potentials, where the regularization parameter is chosen by L-curve method.

We then implemented our inverse and forward models to solve ECG problems in both a concentric spherical geometry and a realistic heart-torso geometry, and investigated the effect of mesh resolution on model results. Experimental results show the accuracy of inverse and forward solutions for ECG problems improves as the mesh resolution increases. Specifically, the relative error in the inverse solution decreased from 30% to 17% when the number of mesh elements triangulating the two spheres increased from 24 to 400 in a concentric spherical geometry, and that decreased from 26% to 16% when the number of mesh elements triangulating the heart surface increased from 136 to 546 in the realistic torso-heart geometry.

REFERENCES

[1] F. Dawoud, G.S. Wagner, G. Moody, and B.M. Horáček, "Using inverse electrocardiography to image myocardial infarction—reflecting on the 2007 PhysioNet/Computers in Cardiology Challenge," *Journal of Electrocardiology*, vol. 41, no. 6, pp. 630-635, 2008.

[2] R.C. Barr, M. Ramsey, and M.S. Madison, "Relating Epicardial to Body Surface Potential Distributions by Means of Transfer Coefficients Based on Geometry Measurements," *IEEE Transactions on Biomedical Engineering*, vol. BME-24, no. 1, pp. 1-11, 1977.

[3] B.M. Burton et al., "A toolkit for forward/inverse problems in electrocardiography within the scirun problem solving environment," in *Conf Proc IEEE Eng Med Biol Soc*, Boston, MA, 2011, pp. 267-270.

[4] J.C. de Munck, T.J.C. Faes, and R.M. Heethaar, "The Boundary Element Method in the Forward and Inverse Problem of Electrical Impedance Tomography," *IEEE Transactions on Biomedical Engineering*, vol. 47, no. 6, pp. 792 - 800, 2000.

[5] P.C. Hansen, "REGULARIZATION TOOLS: A Matlab package for analysis and solution of discrete ill-posed problems," *Numerical Algorithms*, vol. 6, no. 1, pp. 1-35, 1994.

[6] P. C. Hansen, "The L-Curve and its Use in the Numerical Treatment of Inverse Problems," in *Computational Inverse Problems in Electrocardiology*, P. Johnston, Ed.: WIT Press, 2000, pp. 119-142.

[7] M. J. Peters and H. J. Wieringa, "The influence of the volume conductor on electric source estimation," *Brain Topography*, vol. 5, no. 4, pp. 337-345, 1993.

[8] A. L. Goldberger et al., "PhysioBank, PhysioToolkit, and PhysioNet: Components of a New Research Resource for Complex Physiologic Signals," *Circulation*, vol. 101, no. 23, pp. e215-e220, 2000. https://physionet.org/challenge/2007/

[9] D. Yu, D. Du, H. Yang, and Y. Tu, "Parallel computing simulation of electrical excitation and conduction in the 3D human heart," *Proceedings of 2014 IEEE Engineering in Medicine and Biology Society Conference (EMBC)*, pp. 4315 - 4319, August 26-30, 2014, Chicago, IL, United States.